Journal of Solid State Chemistry 293 (2021) 121756

Contents lists available at ScienceDirect

Journal of Solid State Chemistry

journal homepage: www.elsevier.com/locate/jssc

Mechanochemical synthesis of the NiSn, CuSn bimetallic and NiCuSn trimetallic nanocomposites using various types of additives

Katalin Musza [a,b], Márton Szabados [a,b], Adél Anna Ádám [a,b], Péter Bélteky [c], Zoltán Kónya [c,d], Ákos Kukovecz [c], Pál Sipos [b,e], István Pálinkó [a,b,*]

[a] Department of Organic Chemistry, University of Szeged, Dóm tér 8, Szeged, H-6720, Hungary
[b] Material and Solution Structure Research Group and Interdisciplinary Excellence Centre, Institute of Chemistry, University of Szeged, Aradi vértanúk tere 1, Szeged, H-6720, Hungary
[c] Department of Applied and Environmental Chemistry, University of Szeged, Rerrich B. tér 1, Szeged, H-6720, Hungary
[d] MTA-SZTE Reaction Kinetics and Surface Chemistry Research Group, Rerrich B. tér 1, Szeged, H-6720, Hungary
[e] Department of Inorganic and Analytical Chemistry, University of Szeged, Dóm tér 7, Szeged, H-6720, Hungary

ARTICLE INFO

Keywords:
CuSn−NiSn−NiCuSn metals and intermetallics
Surfactant/additive-assisted mechanochemical processing
X-ray diffraction
Scanning and transmission electron microscopies
Dynamic light scattering
Optical and textural analysis

ABSTRACT

Ni-Cu-Sn nanocomposite was prepared for the first time, in the mechanochemical way complementing with the investigation of milled Cu-Sn and Ni-Sn systems using grinding additives. Several chemicals were examined like NaCl, PVP, CTAB, SDS, oleylamine, *n*-heptane, ethylene and polyethylene glycol. X-ray diffractometry attested the varying effects of the additives on the quality and quantity of the milling end-products: in several cases complete or partial mechanical alloying occurred, while in some instances, the segregation of the starting materials were also observed verified by spatially-resolved energy dispersive X-ray analysis. Dynamic light scattering measurements revealed the efficacy of additive amounts used on particle size reduction and size distribution of the milled bimetallic and trimetallic solids. For the Ni-Cu-Sn nanocomposites, the average solvodynamic diameters varied in the range 180–700 nm with 0.21–0.48 polydispersity values. The application of CTAB and PVP resulted in aggregated nanoparticles under 100 nm size in significant amounts verified by the transmission electron microscopy images. The analysis of the surface plasmon resonance bands of the nanocomposites indicated the presence of the Cu(I) oxide phase, while the calculated textural parameters increased up to 5 and 24 m^2/g and 0.01–0.05 cm^3/g specific surface area and total pore volume values, respectively, compared to the 0.8 m^2/g and 0.002 cm^3/g of the milling in the absence of additives.

1. Introduction

Objects, which are of 1 and 100 nm size in at least one dimension, are called nanoparticles (NPs). It is well-known that the chemical and physical properties of NPs are widely different from those of the bulk materials. Nanopowders can be defined as a subclass of NPs: they are powdered elements or compounds in which individual particles fall (or are crystalline) in the nanometer scale [1]. The advantageous properties of nanopowders and even the nanocomposites (in which at least one of the phases is in the nanometric dimension) comprising of elemental metals are associated with their nanometric size [2], as the surface to volume ratio is large, and the number of surface atoms is comparable to that of the atoms inside the NP [3,4]. This, among others, results in the alteration of surface energy [5], and in several mechanical properties [6] and increases the reactivity of the nanocomposites. Nanopowders are used in a large variety of applications including surface-enhanced spectroscopy and microscopy, light harvesting, solar cell fabrication [7–10], catalysis [11], preparation of nanocomposites and sensors [12–14] as well as medical diagnoses and treatments [15–17].

The actual selection of the preparation technique is challenging task in itself. Various preparation ways result in NPs/nanocomposites with fundamentally different morphology, i.e., structure and size, and in association with this, stability and physico-chemical properties of the products. It is known well that the major branches of NP fabrications are the bottom-up and the top-down techniques. The most commonly used top-down techniques are mechanical milling [18,19], laser ablation [20], inert gas condensation [21], physical vapour deposition [22], laser pyrolysis [23] and flame pyrolysis [24].

* Corresponding author. Department of Organic Chemistry, University of Szeged, Dóm tér 8, Szeged, H-6720, Hungary.
E-mail address: palinko@chem.u-szeged.hu (I. Pálinkó).

https://doi.org/10.1016/j.jssc.2020.121756
Received 5 July 2020; Received in revised form 24 September 2020; Accepted 27 September 2020
Available online 30 September 2020

In the present contribution, the mechanochemical route was used for the fabrication of nanocomposites. The definition of mechanochemistry, according to Heinecke, includes chemical and/or physical transformation employing the effect of mechanical energy input [25]. During the milling process, unusual transformations can also occur in the localized spots with extreme conditions (>5000 K, several tens of atmospheres with extremely short $<10^{-7}$s relaxation times). New materials can be mechanochemically obtained from precursors by mechanical activation or they can be produced *via* modifying structures, which already exist [26]. Mechanochemistry is known to be advantageous against solvent-based synthesis methods, for the latters are known to be (among others) unsustainable [27,28]. Furthermore, there are several and easily available, simple to set up, moderately priced instruments with their own specific operation characters to perform the mechano- (rolling, mixer or planetary mill) treatments making them suitable for lab-scale applications.

One can find a considerable number of examples in the literature where mechanochemistry was employed in the synthesis of metallic NPs or nanocomposites. For instance, monometallic Ni and bimetallic Ni-Cu NPs where synthesized from commercial nickel powder using high-energy ball milling [29]. From copper powder, Cu [30] and Cu_2O [31] NPs can also be prepared this way. Examples are also found for the mechanochemical preparation of other bimetallic, e.g., Fe-Cu [32] and Ni-Fe [33], NPs. Perhaps, the most intensely studied bimetallic system is the Cu-Ni one [34–38], and the Cu-Sn and Ni-Sn systems are much less explored. However, Pithakratanayothin et al. could synthesize Ni/Cu-Sn intermetallics in an attrition mill [39], and similar nanocomposites were prepared investigating the short mechanical activation of Cu-Sn/In and Ni-Sn/In systems [40]. Moreover, the synthesis of Sn-rich cobalt- and nickel-containing intermetallics were published using mechanical alloying [41,42], as well as a rare solid-liquid ball milling technique for the preparation of Cu-Sn and Cu-Ni-Sn intermetallic powders [43].

Not surprisingly, the preparation and the properties of trimetallic NPs/nanocomposites are largely unexplored areas. The most probable reason of this is associated with the difficulties of creating a suitable chemical environment in which all the three metals are simultaneously present in elemental state to form nanometric size objects. One of the rare literature examples includes the deposition of Ag *via* reduction to the surface of a bimetallic Au-Pt NP resulting in a product with core-shell structure [44]. In the same publication, the deposition of Rh on bimetallic Pd-Ag was also successfully managed using this synthesis strategy. Employing the gas-phase method, Au-Pd-Pt NPs were synthesized [45], while Fe-Ni-Ce NPs were reported to be prepared by coprecipitation [46]. Mechanochemical method was used for the preparation of Ru-Sn-Mo and Ru-Se-Mo NPs in the presence of isopropanol additive resulting in the formation of the physical mixtures of various bimetallic alloys and pure metals [47].

Using inorganic or organic additives, the process of mechanical alloying and cold-welding can be minimized by masking metal-to-metal contacts and providing with optimized balance between the fracture and coalesce of the particles [48,49]. In spite of the received increasing attention of the use of milling additives in the last decades, the scale of the frequently applied substances are quite narrow; short-chain alcohols and stearates [50], inorganic sodium salts [51], oleic acid/oleylamine [52] and hexane-heptane-benzene compounds [49,53] are the most studied ones. Therefore, during this work, the main goal was the mechanochemical preparation of bi- (Cu-Sn and Ni-Sn) and trimetallic (Cu-Ni-Sn) nanocomposites *via* ball milling using commercial metal powders as starting materials. In addition, we attempted to establish the effect of the quality and the quantity of various additives (investigating the most often used surfactants in wet chemistry like CTAB, SDS and PVP) on the products obtained using a set ensemble of previously optimized instrumental parameters.

2. Experimental

2.1. Materials

Copper powder (<75 μm granule size in face-centred cubic structure), nickel powder (<50 μm, face-centred cubic), *n*-heptane and sodium dodecyl sulphate (SDS) were purchased from Sigma-Aldrich (USA). Tin powder (<44 μm, tetragonal β phase) and polyvinylpyrrolidone (PVP, average mol wt. 40000) were acquired from Alfa Aesar GmbH (Germany). Ethylene glycol, sodium chloride, cetyltrimethylammonium bromide (CTAB), absolute ethanol were supplied by the VWR International (EU). The cis 1-amino-9-octadecene (oleylamine) was obtained from Acros Organics (USA) and the polyethylene glycol 400 from Merck KGaA (Germany). All chemicals were of 99%+ purity, and no further purification was required, save the CTAB ($C_{19}H_{42}BrN \geq 97.0\%$) and the oleylamine (C18-content 80–90%).

2.2. Mechanochemical process for the synthesis of the bi- and trimetallic nanocomposites

The mechanochemical treatments were performed in a Retsch MM 400 mixer mill operating with two grinding jars (stainless steel, 50 cm^3 inner volume) and a grinding ball (25 mm diameter and ~60 g, stainless steel) in each jar, under air atmosphere. The ball to powder mass ratio was around 100, the applied grinding frequency (12 Hz) and time interval (2 h) were fixed. The balls impinged from the rounded ends of the jars, which moved in radial oscillations along the horizontal axis resulting in sudden collisions, therefore, the induced mechanical deformations were somewhat different from the circular motion in the commonly used rolling or planetary ball mill [54].

The amount of metal solids were 0.6 g applying 1:1 Cu:Sn, 1:1 Ni:Sn and 1:1:1 Ni:Cu:Sn molar ratios, while the amount of the added surfactants varied in the range of the 50 mm^3 and 500 mm^3 for the liquid additives. For NaCl and the solid surface active agents, the used masses were between 0.5 and 5 wt% of the 0.6 g total mass of the metal particles. After milling, the samples were washed with distilled water and ethanol, collected on 0.22 μm filters, dried at 60 °C and stored under N_2.

2.3. Applied techniques for the structural characterization

The powder X-ray diffractograms were recorded on a Rigaku Miniflex II instrument using $Cu_{K\alpha}$ ($\lambda = 1.5418$ Å) radiation in the $\Theta = 5-80°$ range with 4°/min scan speed. The reflections were identified on the normalized diffractograms by the JCPDS−ICDD (Joint Committee of Powder Diffraction Standards − International Centre for Diffraction Data) database. The coherently scattering domain sizes (the smallest undistorted zone − average crystallite sizes) of the Cu_6Sn_5 crystals were calculated by the Scherrer equation fitting Gaussian curves on the first reflections applying 0.9 shape factor. The analysis of the wt% distribution of the phases were performed using the integrated reflection intensities [54].

The morphologies and the sizes of the nanocomposites were investigated by scanning (SEM, Hitachi S-4700 instrument) and transmission (TEM-FEI TECHNAI G220 X-TWIN instrument) electron microscopies at varied magnifications and acceleration voltages. The dispersion of the metal elements were analyzed by energy dispersive X-ray spectroscopy accessory coupled to the scanning electron microscope (EDX, Röntec QX2 spectrometer equipped with Be window).

To map the average solvodynamic diameters and heterogeneity in particle sizes of the solids, a Malvern NanoZS dynamic light scattering (DLS) apparatus operating with a 4 mW helium-neon laser light source (λ = 633 nm) was used. The analyses were performed in back-scattering mode at 173°, the size measuring limit of the instrument was near 6 μm, and the particles were dispersed in ethylene glycol with 1 h

ultrasonic radiation getting 0.1 g/dm^3 concentration.

The registration of the surface plasmon resonance of the metallic particles were done in the range of 225–800 nm using a Shimadzu UV–1650 double beam spectrophotometer with 1 cm cuvette length and 2 nm resolution. The parameters of the analyzed dispersions were the same as used for the DLS measurements.

The N_2 adsorption-desorption isotherms were registered on a Quantachrome NOVA 3000e instrument. The samples were degassed at 200 °C for 3 h in vacuum to clear away the surface-adsorbents. The specific surface areas were estimated by the Brunauer-Emmett-Teller equation from the adsorption branches, while the total pore volumes were calculated with the method of Barett-Joyner-Halenda (BJH) from the desorption branches.

3. Results and discussion

3.1. Preparation of bimetallic CuSn and NiSn nanostructures

The mechanochemical synthesis of the bimetallic nanocomposites was started with the investigation of the effect of the surfactants on the end-products in the milling of Cu and Sn metal powder by X-ray diffractometry. Since the number of the known and even the generally used surfactants are extremely large, the quantity and quality of the additives were varied in wide range using liquid and solid ones (at room temperature), non-ionic (*n*-heptane, ethylene glycol, polyethylene glycol, PVP, oleylamine), anionic (SDS) and cationic (CTAB) surface active agents with low and high molecular weights as well. However, the NaCl is not considered as surfactant, it is generally used as inert grinding media to aid the uniform energy dissipation and to work against aggregation and cold-welding [55]. In the absence of additive and on using *n*-heptane and NaCl (Fig. S1, "S" is the notation used in the Supporting Information), the signal of the exclusive end-product was attributed to the η-bronze intermetallic (Cu_6Sn_5, monoclinic, C2/c space group, 45−1488 numbered JCPDS card), while only the reflections of the Cu (JCPDS#04−0836) and Sn (JCPDS#04−0673) starting materials could be identified after the millings with oleylamine or polyethylene glycol, save the weak sign of the partial oxidation of the Cu into the copper(I) oxide phase at lower polyethylene glycol amounts (under 1 wt%, JCPDS#78−2076) (Fig. S2). In these cases, the quantities of the additives had no influence on the outcome of mechanical treatments. Significantly different behaviour was observed on working with PVP, CTAB, SDS or ethylene glycol; the formation of η-bronze alone or the physical mixture of bronze, copper and tin occurred depending on the quantity and quality of the surfactants. At higher amounts of additives, the predominant phases were the starting metals, and lower amounts favoured to the formation of the η-bronze on using PVP, CTAB or SDS (Fig. S3). Interestingly, reverse tendency could be observed with ethylene glycol: the increasing amounts of the additive aided the generation of the bronze phase (Fig. 1). The calculated values of the Cu_6Sn_5 content were between 22 and 95 wt% (Table S1) depending mainly on the amounts of the additives used, the Sn content diminished under the theoretically minimum (10.5 wt% assuming only the formation of Cu_6Sn_5 phase), while the amount of the unreacted Cu particles were still detectable. These observations could indicate that part of the Sn reagents became amorphous (invisible by X-ray diffractometry) and/or the bronze intermetallic was not formed exclusively with the expected stoichiometric formula, but rather with Sn-rich compositions [56,57].

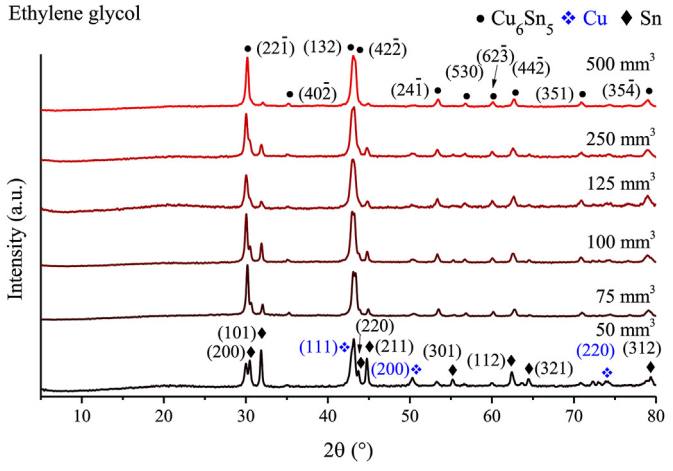

Fig. 1. X-ray diffractometry of the product(s) obtained after the mechanochemical treatment of Cu-Sn mixture applying ethylene glycol milling additive in different amounts.

The work on the Ni-Sn system resulted in the similar tendencies. Two cases were clearly distinguishable (i) solely the reflections of the nickel (JCPDS#04−0850) and tin starting materials were observed on using oleylamine and polyethylene glycol (Fig. S4) and (ii) beside these reflections, some unidentified ones were observed for the additives PVP, CTAB, SDS, ethylene glycol, NaCl or *n*-heptane (Fig. S5). The predominant phases were the tin and nickel on using PVP, CTAB, SDS, ethylene glycol, and only a few signals assigned to the unknown phase/phases were recorded; but, numerous strong unknown reflections appeared on applying *n*-heptane and especially sodium chloride and in the absence of additive, where the reflections of tin particles were even hardly observable. The identification of the new reflections were not possible either assuming the likely formation of metal oxide (or even nitride, carbonate) secondary products or the well-known transformation of the starting face-centred cubic (Cu and Ni) into the hexagonal close packed structure or the tetragonal β phase tin to the diamond cubic α phase (tin pest). Although, several reflections could not be assigned, the signals of the hexagonal Ni_3Sn (35−1362) intermetallic compound were clearly separated with largely similar lattice parameters (Table S2). Under 45° 2θ the weak reflections remained unidentified in spite of our best efforts, but the intense signals appearing around 30° and 42° 2θ could presumably be connected to the formation of intermetallics with lower Ni content ($Ni_{1.52}Sn$ [58], $Ni_{2.7}Sn_2$ [59], $Ni_{3.08}Sn_4$ [60], $Ni_{0.62}Sn_5$ [61]). The generation of these solids may be verified by the slower consumption of the nickel starting reagents compared to that the tin particles had. Using *n*-heptane and NaCl additives, the reflections of the nickel phase were still well-observable beside the largely disappearing signals of the tin reagent in the diffractograms (Fig. S5). Mulas et al. experienced the formation of similar Sn-rich Ni-Sn intermetallics using single-ball mixer milling without any additives [41]. Moreover, suggested by the experimental results of the Cu and Sn solids milled with NaCl and *n*-heptane, where the formation of the Cu_6Sn_5 intermetallic compound was mainly favoured, the generation of a NiSn intermetallic system thought to be a highly conceivable solution. The reverse tendency between the PVP−CTAB−SDS and ethylene glycol was also observed during the milling of Ni-Sn powder (the increasing amount of ethylene glycol aided the generation of the intermetallic compounds); however, with the other additives, the reflections of the intermetallic alloys intensified when their amounts decreased.

Interestingly, from the liquid additives, significantly larger amounts were necessary (>5%, calculated in wt% compared to total mass of the starting metal particles) than from the solids to avoid the formation of thin foil on the internal surface of grinding jars from the ductile copper and tin particles. This phenomenon could be inhibited with only 1 mm^3 oleylamine, ethylene glycol or dimethyl sulfoxide when copper was milled [60]; however, for these bimetallic systems, at least 50 mm^3 of these liquids were needed. In addition, the average crystallite sizes of the formed η-bronze intermetallic showed growing tendency from 19 to 39 nm with the mass of the additives used (23 nm for the milling without additive), and for the *n*-heptane and ethylene glycol (applied in higher amounts), the curves went through maxima (Fig. S6).

Since the mechanical deformations (mainly plastic deformations) are induced largely by impacts with random magnitude and intensity, the

evolution of specific morphologies are quite rare, as it was attested by the electron microscopic images: only planar and highly aggregated particles (flattened by the mechanical compressive forces) with smooth edges could be observed (Fig. 2). In spite of the lower than atomic resolution of SEM, from the EDX elemental maps, one could verify visually the formation of the various end-products; the generated η-bronze intermetallic (in the presence of NaCl), the physical mixture of the intact starting materials (in the presence of oleylamine), and the mixture of the intermetallics and starting Cu and Sn particles could be distinguished well (in the presence of ethylene glycol). For the NiSn solids, SEM-EDX measurements revealed amorphous, rounded particles, the elemental distribution maps verified the formation of the NiSn intermetallic alloy/alloys demonstrated with NaCl and PVP milling additives and the physical mixture of the Ni and Sn starting materials (oleylamine) (Fig. S7). Furthermore, in all cases, the elemental analysis did not register the presence of the iron atoms as possible contaminant from the amortization of the grinding jars or balls. TEM analysis revealed Cu/Sn grains under micron sizes in agreement with DLS measurements (detailed below). Moreover, at the highest magnifications, separate nanoparticles under 50 nm were also observable in the aggregates (Fig. 3).

For the dynamic light scattering measurements, the milled Cu-Sn systems, in the presence of additives, formed light-grey semi-transparent and non-settling dispersions after 1 h ultrasonic stirring in ethylene glycol. The number-weighed size distribution curves of the ground samples displayed mainly unimodal character (not shown), the size of the aggregated crystallites had only one maximum. The liquid and solid additives displayed well-separated behaviour independently from the quality of the evolved end-products. With NaCl, PVP, SDS and CTAB, the average solvodynamic diameters remained in small range (between 540 and 230 nm), and the polydispersity indices (PDI) were under 0.6. Increasing amounts of the additives resulted in slightly decreased sizes and PDI values, except with SDS, when the lowest diameters were measured at 1.5 and 2 wt%.

For the liquid additives, the influence on the aggregation tendency was more remarkable, the values of the average solvodynamic diameters as well as the PDI values varied from 1600 to 190 nm and from 0.76 to 0.16, respectively. Oleylamine, ethylene and polyethylene glycol aided the aggregation and/or the cold-welding of metal particles at higher amounts; the lowest diameters were measured for the 50 mm^3 volume added. *n*-Heptane showed different behaviour, but similar to NaCl and PVP. The smallest diameters were detected when heptane was used in the largest amount.

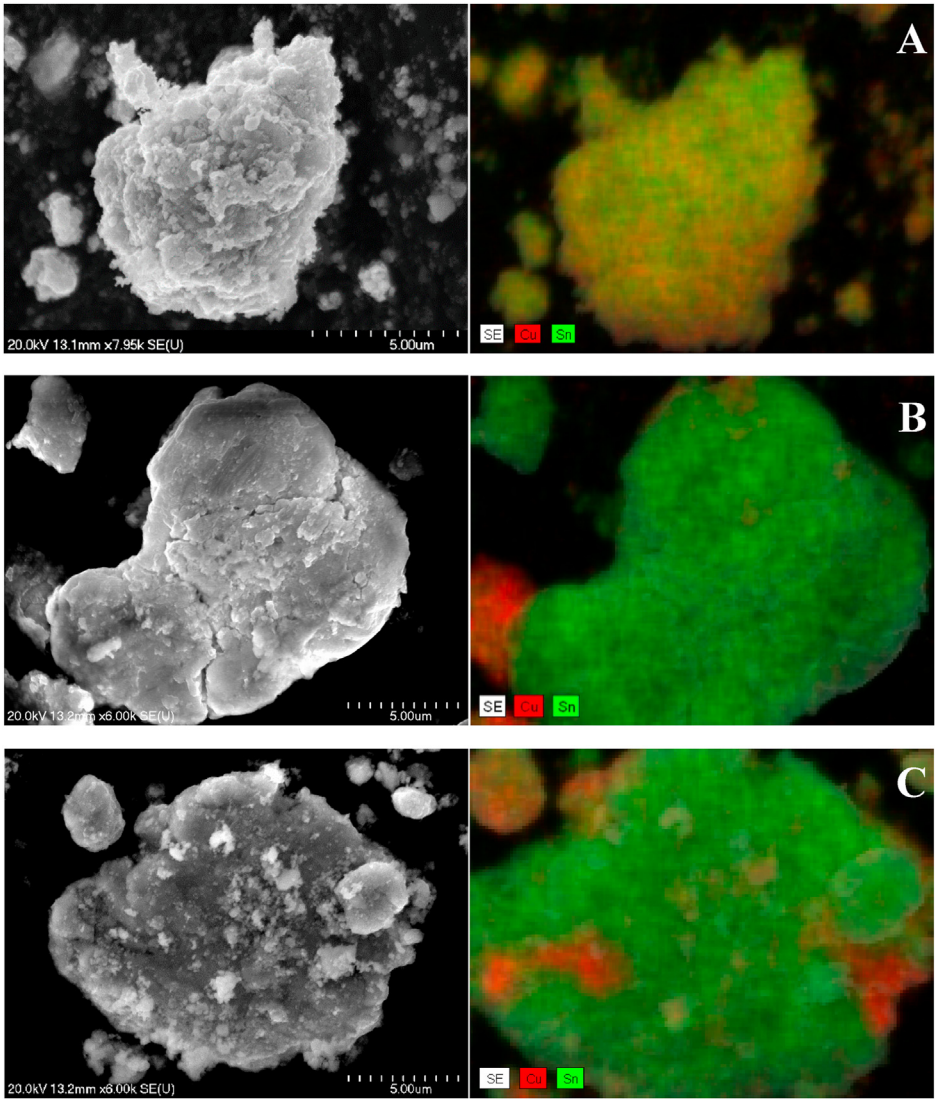

Fig. 2. SEM images and the corresponding elemental distribution maps derived from energy dispersive X-ray analysis of the milled Cu-Sn powders with 5 wt% NaCl (A), 50 mm^3 oleylamine (B) and ethylene glycol (C).

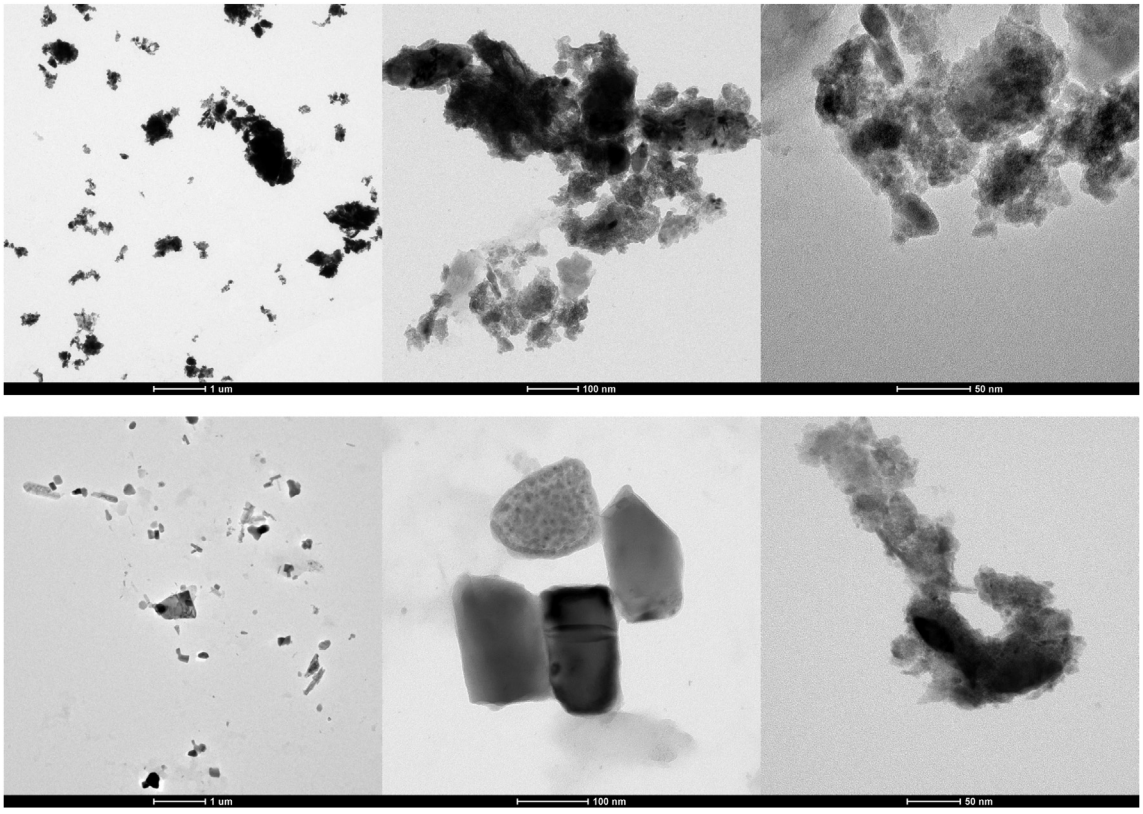

Fig. 3. TEM images of the milled Cu-Sn powders with 5 wt% PVP (upper row, 1 μm, 100 nm, 50 nm scale bars), 500 mm^3 *n*-heptane (bottom row, 1 μm, 100 nm, 50 nm scale bars).

3.2. Synthesis of the NiCuSn trimetallic system

During the syntheses, the experimental experiences were used obtained in the works with the CuSn and the NiSn bimetallic materials. To obtain particles with the smallest extent of aggregation (highlighted in Table 1), the amount of the used additives were chosen according to the DLS measurements (Fig. 4). From ethylene glycol, 125 mm^3 were applied, for the similarly small particles, but with the lowest PDI values. The revealed behaviour of the additives was the same for the trimetallic system as well: the application of oleylamine and polyethylene glycol resulted in total segregation of the starting reagents, the XRD patterns only registered the physical mixture of the Ni, Cu and Sn solids, while with NaCl and *n*-heptane and in the absence of additive, the Cu and Sn particles formed the Cu_6Sn_5 phase excluding nickel. For the rest of the surfactants, the reflections of the starting reagents and the η-bronze were also observable in various phase distributions (Table S1). However, in most instances, the evolution of the cupronickel intermetallic ($Cu_{0.81}Ni_{0.19}$ JCPDS#47−1406) could not be probed, because their reflections are in the same position as those of the Cu particles. Working with NaCl, *n*-heptane or without additive, the absence of the copper reflection allowed us to rule out the formation of the CuNi intermetallic as well [62]. Moreover, the signals of NiSn intermetallics could not be detected either indicating that the generation of the Cu_6Sn_5 intermetallic compound is preferred in the all cases. For the binary and ternary systems, the lattice parameters (Table S1) of the formed Cu_6Sn_5 phases were similar to the ones reported in the literature [63], but changed in a relatively wide range due to the generated lattice stress from the disordering/fracturing effect of the mechanochemical treatments [64]. When Ni was present, these parameters did not show clear changes not registering the dissolution of the nickel atoms into the Cu_6Sn_5

Table 1
Dispersion dimensions of the Cu-Sn bimetallic system (average solvodynamic diameter – $Z_{avg.}$, polydispersity index – PDI).

Amount of the additives (wt.%)	NaCl		PVP		SDS		CTAB	
	$Z_{avg.}$ (nm)	PDI	$Z_{avg.}$ (nm)	PDI	$Z_{avg.}$ (nm)	PDI	$Z_{avg.}$ (nm)	PDI
0.5	520 ± 35	0.41	470 ± 40	0.49	310 ± 20	0.29	440 ± 35	0.30
1.0	480 ± 30	0.46	540 ± 30	0.54	315 ± 30	0.28	460 ± 30	0.59
1.5	250 ± 20	0.34	470 ± 20	0.59	250 ± 10	0.29	535 ± 40	0.35
2.0	255 ± 15	0.35	365 ± 40	0.44	250 ± 20	0.27	305 ± 5	0.43
3.0	240 ± 15	0.35	380 ± 35	0.36	335 ± 15	0.20	320 ± 10	0.48
5.0	230 ± 10	0.33	270 ± 5	0.33	310 ± 20	0.19	270 ± 20	0.27
Amount of the additives (mm^3)	Oleylamine		Ethylene glycol		Polyethylene glycol		*n*-Heptane	
	Z_{avg} (nm)	PDI	Z_{avg} (nm)	PDI	Z_{avg} (nm)	PDI	Z_{avg} (nm)	PDI
50	440 ± 40	0.34	285 ± 10	0.21	260 ± 5	0.24	240 ± 20	0.35
75	550 ± 55	0.37	280 ± 25	0.24	365 ± 15	0.25	390 ± 20	0.37
100	770 ± 65	0.35	330 ± 20	0.21	490 ± 40	0.5	310 ± 15	0.34
125	575 ± 20	0.31	240 ± 10	0.29	550 ± 30	0.52	225 ± 5	0.16
250	940 ± 90	0.48	490 ± 35	0.21	1400 ± 190	0.61	210 ± 10	0.22
500	1500 ± 220	0.70	610 ± 40	0.30	1600 ± 300	0.76	190 ± 10	0.23

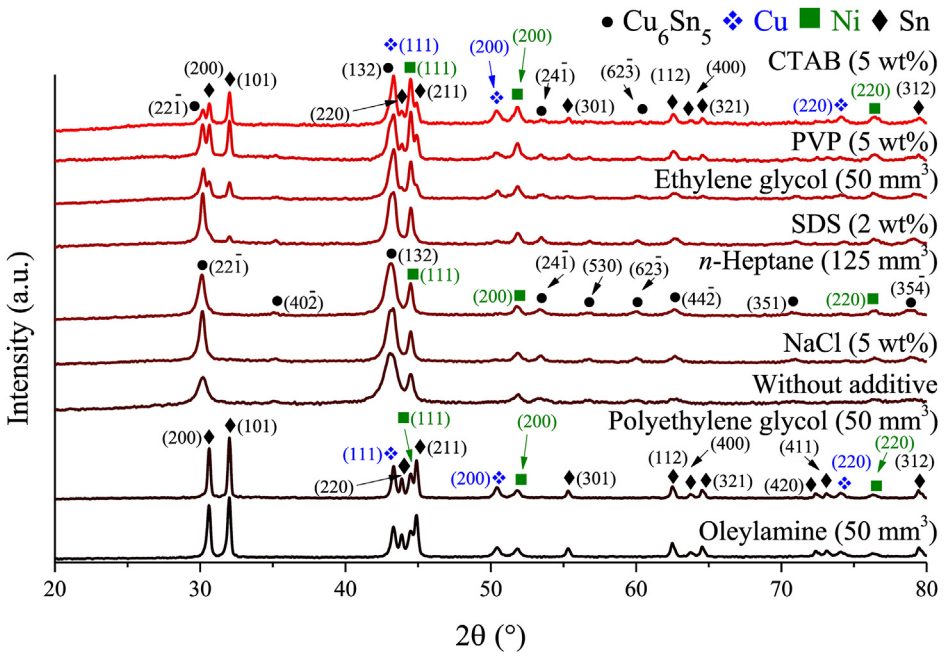

Fig. 4. XRD patterns of the milled Ni-Cu-Sn powders without and using various additives in amounts determined previously.

intermetallic [65,66]. In addition, the phase distribution data revealed largely uniform and same as the initial (24.3 wt% in the starting reagents) content of the unreacted Ni; nevertheless, the incorporation of the nickel atoms cannot be ruled out entirely. Due to the similar physicochemical properties of the Cu and Ni atoms, in minute amount, the formation of the NiCuSn intermetallic can be presumable.

To sum up, X-ray diffractometry results of the CuSn, NiSn and NiCuSn systems revealed that the smaller NaCl and *n*-heptane molecules could not prevent the mechanical alloying of the starting materials as it was always recorded using no additive. Presumably, the molecules with longer hydrocarbon chains and/or polar groups would adsorb on the surface of the particles forming protective layer and sterically/electrically inhibiting the fusion of the starting metals. Since the surface of the metal particles did not have specific charge, the ionic character of the surfactants did not have significant influence on the quality of the end-products. Oleylamine and polyethylene glycol were extremely efficient in preserving the starting materials, while this was highly dependent on the applied amounts of the PVP, CTAB, SDS or ethylene glycol.

3.3. *Dynamic light scattering and electron microscopic investigations*

The DLS curves of the NiCuSn nanocomposites had unimodal distribution with average solvodynamic diameters fluctuating in wide scale; however, the PDI values remained relatively similar (Fig. 5, Table 2). Compared to the curve obtained for the blank sample, the size of the aggregates could be reduced successfully applying milling additives, except in the presence of SDS. In most cases, the particles were in the 100 and 1000 nm range, but with PVP and CTAB, ~ 11% and ~19% of the particles, respectively, were smaller than 100 nm. The TEM images verified the nanometer size of the NiCuSn powders derived from the DLS measurements. At high magnifications, several particles were recorded under 100 nm aggregated into micron sized formations (Fig. 6).

On the SEM images, the already seen rounded planar morphology was observed, and the EDX elemental maps visualize the deviation between the generation of bronze intermetallic and the simple physical mixture of the three starting materials (Fig. S8). Interestingly, a slight difference was observed regarding the position of the nickel particles around the CuSn intermetallic alloy. In the presence of SDS, EG, CTAB and PVP, where the formation of the bronze intermetallic was less favoured, and the

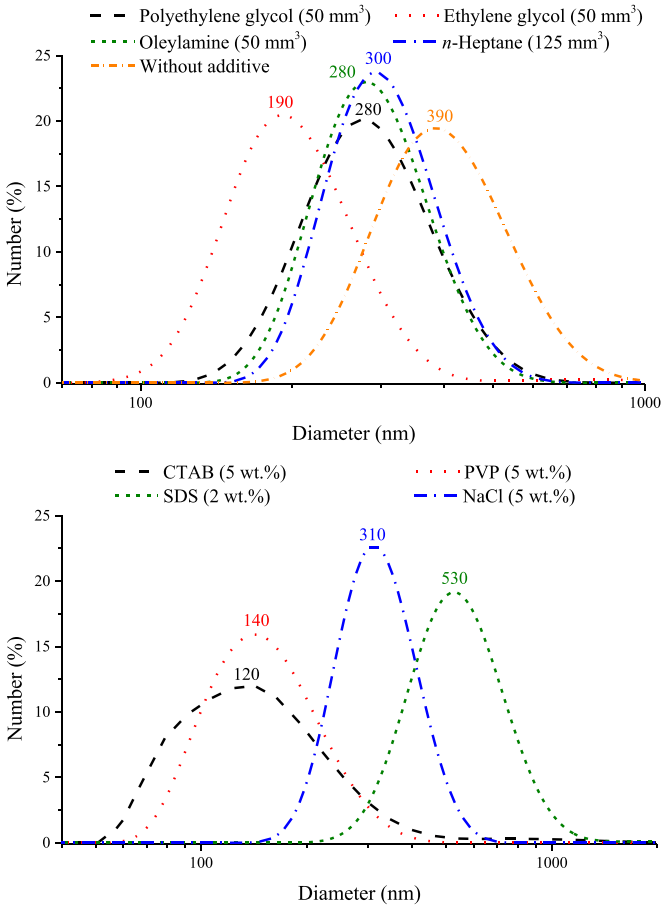

Fig. 5. The number-weighed size distribution curves of the prepared NiCuSn nanocomposites in the absence of or applying various milling additives (the numbers represent the predominant solvodynamic diameters).

Table 2
Textural, size and heterogeneity parameters of the NiCuSn trimetallic systems prepared.

Milled Ni, Cu and Sn powders with different additives	Specific surface area (m^2/g)	Total pore volume (cm^3/g)	Average solvodynamic diameter (nm)	Poly-dispersity index
Without additive	0.8	0.002	500 ± 60	0.30
CTAB (5 wt%)	19.3	0.027	245 ± 15	0.48
PVP (5 wt%)	18.6	0.046	180 ± 10	0.21
Ethylene glycol (50 mm^3)	23.7	0.029	250 ± 45	0.33
SDS (2 wt%)	5.4	0.009	700 ± 65	0.31
n-Heptane (125 mm^3)	5.2	0.009	320 ± 20	0.25
NaCl (5 wt%)	12.4	0.021	370 ± 45	0.28
Polyethylene glycol (50 mm^3)	6.4	0.012	410 ± 30	0.44
Oleylamine (50 mm^3)	5.1	0.013	315 ± 10	0.26

reflections of the Cu and Sn phases were also detected, beside the Ni particles, the signal of the latter element was located separately around the bronze on the elemental maps (Fig. S8). While the distribution of the Ni elements were more uniform covering completely the atoms of the Cu_6Sn_5 intermetallic for the work without any and with NaCl and *n*-heptane milling additives where the end-products consisted of largely the bronze and nickel solids, the formation of the intermetallic phase was the most favoured (Fig. 7).

3.4. UV–visible absorption, specific surface area and total pore volume analysis

The reach of the nanoscopic scale allowed us to investigate the optical properties of the milled NiCuSn powders *via* the identification of the localized surface plasmon resonance bands in the UV–visible spectra. Since the charge density oscillations are highly dependent on the size and shape of the metallic nanoparticles, the recorded bands were relatively broad; nevertheless, three peaks were clearly observable around 265, 490 and 615 nm. The first signal was attributed to the presence of nickel nanoparticles [67,68] for all solids (not shown), the last two were derived from the Cu_2O and Cu nanocrystals [69,70] detected clearly for the nanocomposites milled with ethylene glycol, polyethylene glycol, NaCl and especially with CTAB or PVP (resulting in the lowest solvodynamic diamaters) (Fig. S9). The X-ray diffractograms did not show the formation of copper(I) oxide phase, hence these crystals could be largely in amorphous form and/or in minute amount generated on the surface of the copper particles or even originated from the Cu starting reagents.

Since the presence of the Cu_2O component could be a key factor regarding the catalytic potential of the NiCuSn nanoparticles, their textural features were also determined. Even though the phase distribution of the milled solids were different, they all displayed Type IV isotherms mainly with H2 hysteresis loops according to the IUPAC classification [71] indicating disordered mesopores structure with less defined size and shape distribution of the pores (Fig. S10). The solids prepared with PVP, polyethylene glycol and oleylamine showed slightly different isotherms, the registered hysteresis loops were narrower, and their shapes were closer to the curves of H3 and H4 types indicating the evolution of the slit-like pores, too. The isotherm of the solid prepared without additive was similar to those obtained in the presence of polyethylene glycol or oleylamine, but with broader hysteresis loop, presumably as sign of the larger amount of the smaller pores. The obtained values for the specific surface areas and total pore volumes were largely similar and were in a narrow range; the powders containing the maximal four phases (Cu_6Sn_5, Ni, Cu, Sn particles) attested the largest textural parameters, moreover, the application of milling additives could significantly enhance these values in all instances (Table 2).

4. Conclusions

The surfactant/additive-assisted mechanical treatment proved to be a simple and convenient technique to prepare CuSn, NiSn and NiCuSn metallic nanocomposites from commercially available starting metallic particles even in the large scale. While the quantity of the additives had varying influence on the size and size distribution of the frittered particles depending on the composition of the starting materials as well, the effect of their quality brought about three synthesis ways towards the different milling end-products. On the basis of the experimental data obtained with the CuSn, the NiSn and the NiCuSn systems, in all cases the following observations were made (i) independently from the amount of the additives used in the investigated range, the oleylamine and polyethylene glycol inhibited the mechanical alloying, i.e. the starting materials could be preserved in separated forms, (ii) the application of NaCl and *n*-heptane molecules could not hinder the formation of the intermetallic phases as it always occurred in the absence of additive, (iii) the outcome of the millings with PVP, CTAB, SDS and ethylene glycol was highly dependent on the quantity of the applied additives, increasing amounts favoured the formation of the intermetallic compounds for the ethylene glycol, while with PVP, CTAB and SDS the reverse tendency was observed: with higher amounts, the starting materials could be kept separated.

CRediT authorship contribution statement

Katalin Musza: Writing - original draft. **Márton Szabados:** Conceptualization, Supervision, Validation. **Adél Anna Ádám:** Methodology. **Péter Bélteky:** Methodology. **Zoltán Kónya:** Methodology. **Ákos Kukovecz:** Methodology. **Pál Sipos:** Supervision, Funding acquisition, Writing - review & editing. **István Pálinkó:** Conceptualization, Supervision, Validation, Writing - original draft.

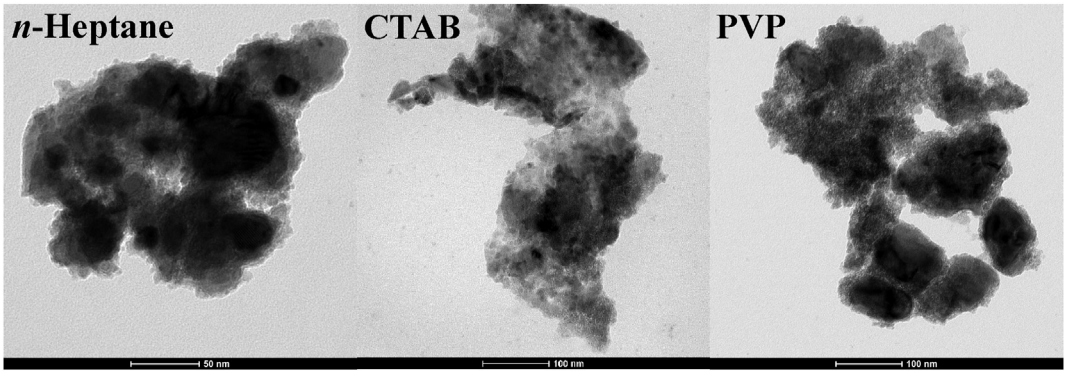

Fig. 6. TEM images of the prepared NiCuSn nanocomposites milled with 125 mm^3 *n*-heptane (50 nm scale bars), 5 wt% CTAB and PVP (100 nm scale bars).

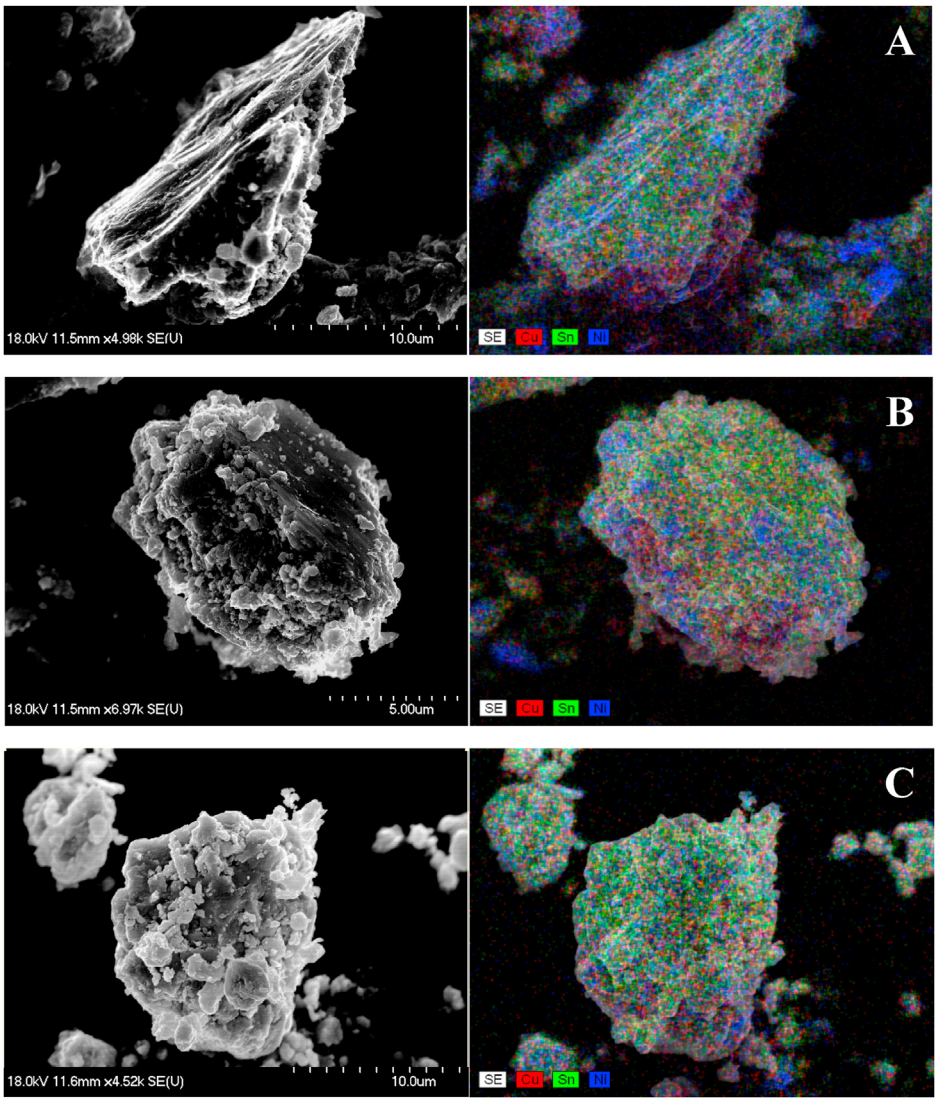

Fig. 7. SEM images and the corresponding elemental distribution maps registered by energy dispersive X-ray analysis of the Ni-Cu-Sn powders milled with 5 wt% NaCl (A) and 125 mm^3 *n*-heptane (B) and without additive (C).

Declaration of competing interest

The authors have no conflicting interests of any kind.

Acknowledgement

This work was supported by the European Union and the Hungarian government through grant GINOP-2.3.2-15- 2016-00013. The financial help is highly appreciated.

Appendix A. Supplementary data

Supplementary data to this article can be found online at https://doi.org/10.1016/j.jssc.2020.121756.

References

[1] J. Wang, S. Wu, X.-K. Suo, H. Liao, The processes for fabricating nanopowders in advanced nanomaterials and coatings by thermal spray, in: Ch. 2 The Processes for Fabricating Nanopowders, 2019, pp. 13–25, https://doi.org/10.1016/B978-0-12-813870-0.00002-4.

[2] V. Pareek, A. Bhargava, R. Gupta, N. Jain, J. Panwar, Synthesis and applications of noble metal nanoparticles: a review, Adv. Sci. Eng. Med. 9 (2017) 527–544, https://doi.org/10.1166/asem.2017.2027.

[3] B.Y. Xia, P. Yang, Y. Sun, Y. Wu, B. Mayers, B. Gates, Y. Yin, F. Kim, H. Yan, One-dimensional nanostructures: synthesis, characterization, and applications, Adv. Mater. 15 (2003) 353–389, https://doi.org/10.1002/adma.200390087.

[4] M.I. Din, A. Rani, Recent advances in the synthesis and stabilization of nickel and nickel oxide nanoparticles: a green adeptness, Int. J. Anal. Chem. 4 (2016) 1–14, https://doi.org/10.1155/2016/3512145.

[5] D. Vollath, F.D. Fischer, D. Holec, Surface energy of nanoparticles – influence of particle size and structure, Beilstein J. Nanotechnol. 9 (2018) 2265–2276, https://doi.org/10.3762/bjnano.9.211.

[6] M.A. Meyers, A. Mishra, D.J. Benson, Mechanical properties of nanocrystalline materials, Prog. Mater. Sci. 51 (2006) 427–556, https://doi.org/10.1016/j.pmatsci.2005.08.003.

[7] D.J. de Aberasturi, A.B. Serrano-Montes, L.M. Liz-Marzán, Modern applications of plasmonic nanoparticles: from energy to health, Adv. Opt. Mater. 3 (2015) 602–617, https://doi.org/10.1002/adom.201500053.

[8] W.A. Murray, W.L. Barnes, Plasmonic materials, Adv. Mater. 19 (2007) 3771–3782, https://doi.org/10.1002/adma.200700678.

[9] U.Y. Qazi, R. Javaid, A review on metal nanostructures: preparation methods and their potential applications, Adv. Nanoparticles 5 (2016) 27–43, https://doi.org/10.4236/anp.2016.51004.

[10] J. Wang, J.R.M. Butet, A.-L. Baudrion, A. Horrer, G.T. Lévêque, O.J. Martin, A.J. Meixner, M. Fleischer, P.-M. Adam, A. Horneber, Direct comparison of second harmonic generation and two-photon photoluminescence from single connected gold nanodimers, J. Phys. Chem. C 120 (2016) 17699–17710, https://doi.org/10.1021/acs.jpcc.6b04850.

[11] R. Narayanan, M.A. El-Sayed, Shape-dependent catalytic activity of platinum nanoparticles in colloidal solution, Nano Lett. 4 (2004) 1343–1348, https://doi.org/10.1021/nl0495256.

[12] P. Gomez-Romero, Hybrid organic–inorganic materials – in search of synergic activity, Adv. Mater. 13 (2001) 163–174, https://doi.org/10.1002/1521-4095(200102)13:3<163::AID-ADMA163>3.0.CO;2-U.

[13] D. Moura, M.T. Souza, L. Liverani, G. Rella, G.M. Luz, J.F. Mano, A.R. Boccaccini, Development of a bioactive glass-polymer composite for wound healing applications, Opt. Mater. 76 (2017) 224–232, https://doi.org/10.1016/j.msec.2017.03.037.

[14] A.M. Salman, A. Al-Janabi, Ni-NPs doped PVA: an efficient saturable absorber for generation multiwavelength Q-switched fiber laser system near 1.5 μm, Mater. Sci. Eng. C 98 (2019), 109418, https://doi.org/10.1016/j.optmat.2019.109418.

[15] K. Banerjee, S. Das, P. Choudhury, S. Ghosh, R. Baral, S.K. Choudhuri, A novel approach of synthesizing and evaluating the anticancer potential of silver oxide nanoparticles in vitro, Chemotherapy 62 (2017) 279–289, https://doi.org/10.1159/000453446.

[16] O. Pascu, J.M. Caicedo, J. Fontcuberta, G. Herranz, A. Roig, Magneto-optical characterization of colloidal dispersions. Application to nickel nanoparticles, Langmuir 26 (2010) 12548–12552, https://doi.org/10.1021/la1011617.

[17] E. Gross, G.A. Somorjai, Molecular catalysis science: nanoparticle synthesis and instrument development for studies under reaction conditions, J. Catal. 328 (2015) 91–101, https://doi.org/10.1016/j.jcat.2014.12.031.

[18] T. Tsuzuki, P.G. Mccormick, Mechanochemical synthesis of nanoparticles, J. Mater. Sci. 39 (2004) 5143–5146, https://doi.org/10.1023/B:JMSC.0000039199.56155.f9.

[19] T.P. Yadav, R.M. Yadav, D.P. Singh, Mechanical milling: a top down approach for the synthesis of nanomaterials and nanocomposites, J. Nanosci. Nanotechnol. 2 (2012) 22–48, https://doi.org/10.5923/j.nn.20120203.01.

[20] S. Amoruso, G. Ausanio, C. de Lisio, V. Iannotti, M. Vitiello, X. Wang, L. Lanotte, Synthesis of nickel nanoparticles and nanoparticles magnetic films by femtosecond laser ablation in vacuum, Appl. Surf. Sci. 247 (2005) 71–75, https://doi.org/10.1016/j.apsusc.2005.01.054.

[21] S.G. Pandya, D. Shafer, M.E. Kordesch, Extended-area deposition of homogeneously sized nanoparticles using modified inert gas condensation technique, Vacuum 114 (2015) 124–129, https://doi.org/10.1016/j.vacuum.2015.01.019.

[22] S. Veintemillas-Verdaguer, M.P. Morales, C.J. Serna, Continuous production of γ–Fe_2O_3 ultrafine powders by laser pyrolysis, Mater. Lett. 35 (1998) 227–231, https://doi.org/10.1016/s0167-577x(97)00251-6.

[23] C.E. Cross, J.C. Hemminger, R.M. Penner, Physical vapor deposition of one-dimensional nanoparticle arrays on graphite: Seeding the electrodeposition of gold nanowires, Langmuir 23 (2007) 10372–10379, https://doi.org/10.1021/la7016209.

[24] W.Y. Teoh, R. Amal, L. Madler, Flame spray pyrolysis: an enabling technology for nanoparticles design and fabrication, Nanoscale 2 (2010) 1324–1347, https://doi.org/10.1039/c0nr00017e.

[25] G. Heinicke, Tribochemistry, Akademie Verlag, Berlin, 1984, pp. 1–495.

[26] J.L. Howard, Q. Cao, D.L. Browne, Mechanochemistry as an emerging tool for molecular synthesis: what can it offer? Chem. Sci. 9 (2018) 3080–3094, https://doi.org/10.1039/C7SC05371A.

[27] L. Takacs, The historical development of mechanochemistry, Chem. Soc. Rev. 42 (2013) 7649–7659, https://doi.org/10.1039/C2CS35442J.

[28] S.L. James, C.J. Adams, C. Bolm, D. Braga, P. Collier, T. Friščić, F. Grepioni, K.D.M. Harris, G. Hyett, W. Jones, A. Krebs, J. Mack, L. Maini, A.G. Orpen, I.P. Parkin, W.C. Shearouse, J.W. Steed, D.C. Waddell, Mechanochemistry: opportunities for new and cleaner synthesis, Chem. Soc. Rev. 41 (2012) 413–447, https://doi.org/10.1039/c1cs15171a.

[29] N. Chawake, R.S. Varanasi, B. Jaswanth, L. Pinto, S. Kashyap, N.T.B.N. Koundinya, A.K. Srivastav, A. Jain, M. Sundararaman, R.S. Kottada, Evolution of morphology and texture during high energy ball milling of Ni and Ni-5 wt% Cu powders, Mater. Char. 120 (2016) 90–96, https://doi.org/10.1016/j.matchar.2016.08.019.

[30] P. Ding, H. Hou, S. Pu, H. Cao, L. Wang, J. Li, Mechanochemical synthesis for studying the melting of metallic nanoparticles: a case study of copper, Phil. Mag. Lett. 95 (2015) 14–20, https://doi.org/10.1080/09500839.2014.995738.

[31] G.R. Khayati, E. Nourafkan, G. Karimi, J. Moradgholi, Synthesis of cuprous oxide nanoparticles by mechanochemical oxidation of copper in high planetary energy ball mill, Adv. Powder Technol. 24 (2013) 301–305, https://doi.org/10.1016/j.apt.2012.07.006.

[32] J. Eckert, J.C. Holzer, C.E. Krill III, W.L. Johnson, Reversible grain size changes in ball-milled nanocrystalline Fe-Cu alloys, J. Mater. Res. 7 (1992) 1980–1983, https://doi.org/10.1557/JMR.1992.1980.

[33] F. Xu, S. Deng, J. Xu, W. Zhang, M. Wu, B. Wang, J. Huang, G. Yu, Highly active and stable Ni-Fe bimetal prepared by ball milling for catalytic hydrodechlorination of 4-chlorophenol, Environ. Sci. Technol. 46 (2012) 4576–4582, https://doi.org/10.1021/es203876e.

[34] X. Xiao, Z. Zeng, Z. Zhao, S. Xiao, Flaking behavior and microstructure evolution of nickel and copper powder during mechanical milling in liquid environment, Mater. Sci. Eng., A 475 (2008) 166–171, https://doi.org/10.1016/j.msea.2007.04.084.

[35] L. Durivault, O. Brylev, D. Reyter, M. Sarrazin, D. Bèlanger, L. Rouè, Cu–Ni materials prepared by mechanical milling: their properties and electrocatalytic activity towards nitrate reduction in alkaline medium, J. Alloys Compd. 432 (2007) 323–332, https://doi.org/10.1016/j.jallcom.2006.06.023.

[36] J. Guerrero-Paz, D. Jaramillo-Vigueras, Nanometric grain formation in ductile powders by low-energy ball milling, Nanostruct. Mater. 11 (1999) 1123–1132, https://doi.org/10.1016/S0965-9773(99)00403-1.

[37] K.J. Kim, K. Sumiyama, K. Suzuki, Formation of nanocrystalline and amorphous phases in $Cu_{80}P_{20}$, $Ni_{82}P_{18}$ and $Cu_{87}Ni_{13}$ mechanically alloyed systems, J. Non-Cryst. Solids 168 (1994) 232–240, https://doi.org/10.1016/0022-3093(94)90334-4.

[38] I. Ban, J. Stergar, M. Drofenik, G. Ferk, D. Makovec, Synthesis of copper–nickel nanoparticles prepared by mechanical milling for use in magnetic hyperthermia, J. Magn. Magn Mater. 323 (2011) 2254–2258, https://doi.org/10.1016/j.jmmm.2011.04.004.

[39] S. Pithakratanayothin, R. Tongsri, T. Chaisuwana, S. Wongkasemjit, Influences of M–Sn intermetallics (M = Ni, Cu) prepared by mechanical alloying on phenol hydroxylation, Catal. Sci. Technol. 7 (2017) 5413–5421, https://doi.org/10.1039/c7cy00655a.

[40] T.F. Grigor'eva, S.V. Tsybulya, S.V. Cherepanova, G.N. Kryukova, A.P. Barinova, V.D. Belykh, V.V. Boldyrev, Mechanochemical synthesis of metastable solid solutions: phase composition and microstructure evolution, Inorg. Mater. 36 (2000) 143–149, https://doi.org/10.1007/BF02758016.

[41] G. Mulas, F. Delogu, S. Enzo, C. Bonatto-Minella, Structural and mechanistic inferences in the mechanochemical synthesis of nanostructured Ni-Sn and Co-Sn alloys, J. Phys. Conf. Ser. 144 (2009), 012025, https://doi.org/10.1088/1742-6596/144/1/012025.

[42] R. Tongsri, N. Tosangthum, Solid state transformation of non-equilibrium Ni-Sn powder with a eutectic composition, Songklanakarin J. Sci. Technol. 33 (2011) 209–214.

[43] D. Chen, W. Wu, Z. Chen, D. Fu, G. Chen, Preparation for intermetallic powders of Cu-Sn and Cu-Ni-Sn systems via solid-liquid reaction milling technique, Trans. Nonferrous Metals Soc. China 17 (2007) 594–598.

[44] N. Toshima, Capped bimetallic and trimetallic nanoparticles for catalysis and information technology, Macromol. Symp. 270 (2008) 27–39, https://doi.org/10.1002/masy.200851004.

[45] J.-G. Mattei, P. Grammatikopoulos, J. Zhao, V. Singh, J. Vernieres, S. Steinhauer, A. Porkovich, E. Danielson, K. Nordlund, F. Djurabekova, M. Sowwan, Gas-phase synthesis of trimetallic nanoparticles, Chem. Mater. 31 (2019) 2151–2163, https://doi.org/10.1021/acs.chemmater.9b00129.

[46] G. Allaedini, S.M. Tasirin, P. Aminayi, Synthesis of Fe–Ni–Ce trimetallic catalyst nanoparticles via impregnation and co-precipitation and their application to dye degradation, Chem. Pap. 70 (2016) 231–242, https://doi.org/10.1515/chempap-2015-0190.

[47] A. Ezeta-Mejía, J.M. Mora-Hernández, J.M. Hallen-López, E.M. Arce-Estrada, Exploration of trimetallic nanoparticles as electrocatalysts for oxygen reduction, Int. J. Electrochem. Sci. 8 (2013) 2044–2055.

[48] A. Nouri, C. Wen, Surfactants in mechanical alloying/milling: a catch-22 situation, Crit. Rev. Solid State 39 (2013) 81–108, https://doi.org/10.1080/10408436.2013.808985.

[49] K.A. Nazari, A. Nouri, T. Hilditch, The addition of a surfactant at regular time intervals in the mechanical alloying process, J. Alloys Compd. 615 (2014) 47–55, https://doi.org/10.1016/j.jallcom.2014.06.142.

[50] L. Lu, Y.F. Zhang, Influence of process control agent on interdiffusion between Al and Mg during mechanical alloying, J. Alloys Compd. 290 (1999) 279–283, https://doi.org/10.1016/S0925-8388(99)00221-2.

[51] J. Zheng, C.C. Harris, P. Somasundaran, The effect of additives on stirred media milling of limestone, Powder Technol. 91 (1997) 173–179, https://doi.org/10.1016/S0032-5910(96)03236-6.

[52] L. Zheng, A.M. Gabay, W. Li, B. Cui, G.C. Hadjipanayis, Influence of the type of surfactant and hot compaction on the magnetic properties of $SmCo_5$ nanoflakes, J. Appl. Phys. 109 (2011), 07A721, https://doi.org/10.1063/1.3561443.

[53] H. Geng, Y. Ji, X. Feng, J. Zhang, Y. Gao, Y. Yan, W. Wang, F. Su, X. Du, Preparing $Sm_2Fe_{17}C_x$ compound by high-energy ball-milling Sm-Fe alloy in heptane followed by annealing, re-milling and re-annealing, J. Appl. Phys. 111 (2016) 140–145, https://doi.org/10.1016/j.matdes.2016.09.001.

[54] C.R. Hubbard, E.H. Evans, D.K. Smith, The reference intensity ratio, I/Ic, for computer simulated powder patterns, J. Appl. Crystallogr. 9 (1976) 169–174, https://doi.org/10.1107/S0021889876010807.

[55] P. Baláž, M. Achimovičová, M. Baláž, P. Billik, Z. Cherkezova-Zheleva, J.M. Criado, F. Delogu, E. Dutková, E. Gaffet, F.J. Gotor, R. Kumar, I. Mitov, T. Rojac, M. Senna, A. Streletskii, K. Wieczorek-Ciurowa, Hallmarks of mechanochemistry: from nanoparticles to technology, Chem. Soc. Rev. 42 (2013) 7572–7637, https://doi.org/10.1039/C3CS35468G.

[56] G. Zeng, S.D. McDonald, J.J. Read, Q. Gu, K. Nogita, Kinetics of the polymorphic phase transformation of Cu_6Sn_5, Acta Mater. 69 (2014) 135–148, https://doi.org/10.1016/j.actamat.2014.01.027.

[57] C.K. Lin, C.-M. Liu, C. Chen, Formation of Sn-rich phases via the decomposition of Cu_6Sn_5 compounds during current stressing, Mater. Lett. 124 (2014) 261–263, https://doi.org/10.1107/S0021889876010807.

[58] A. Leineweber, O. Oeckler, U. Zachwieja, Static atomic displacements of Sn in disordered NiAs/Ni_2In type HT-$Ni_{1+\delta}Sn$, J. Solid State Chem. 177 (2004) 936–945, https://doi.org/10.1016/j.jssc.2003.09.033.

[59] H. Fjellvåg, A. Kjekshus, Structural properties of Co_3Sn_2, Ni_3Sn_2 and some ternary derivatives, Acta Chem. Scand. 40 (1986) 23–30, https://doi.org/10.3891/acta.chem.scand.40a-0023.

[60] S. Furuseth, H. Fjellvåg, Structural properties of $Ni_{(3+x)}Sn_4$, Acta Chem. Scand. 40 (1986) 695–700, https://doi.org/10.3891/acta.chem.scand.40a-0695.

[61] H. Ying, J. Bai, S. Li, F. Xin, G. Wang, W. Wen, X. Yan, Z. Meng, W.-Q. Han, A New intermetallic NiSn5 phase: induced synthesis, crystal structure resolution, and investigation of its mechanism, J. Phys. Chem. Lett. 10 (2019) 2561–2566, https://doi.org/10.1021/acs.jpclett.9b00704.

[62] K. Musza, M. Szabados, A.A. Ádám, Z. Kónya, Á. Kukovecz, P. Sipos, I. Pálinkó, Ball milling of copper powder under dry and surfactant-assisted conditions – on the way towards Cu/Cu_2O nanocatalyst, J. Nanosci. Nanotechnol. 19 (2019) 389–394, https://doi.org/10.1166/jnn.2019.15784.

[63] C. Wieser, A. Walnsch, W. Hügel, A. Leineweber, The monoclinic lattice distortion of η′-Cu_6Sn_5, J. Alloys Compd. 794 (2019) 491–500, https://doi.org/10.1016/j.jallcom.2019.04.265.
[64] C. Suryanarayana, Mechanical alloying: a novel technique to synthesize advanced materials, Research 10 (2019) 1–17, https://doi.org/10.34133/2019/4219812.
[65] K. Nogita, D. Mu, S.D. McDonald, J. Read, Y.Q. Wu, Effect of Ni on phase stability and thermal expansion of $Cu_{6-x}Ni_xSn_5$ (X = 0, 0.5, 1, 1.5 and 2), Intermetallics 26 (2012) 78–85, https://doi.org/10.1107/S0021889876010807.
[66] E. Nagy, F. Kristály, A. Gyenes, Z. Gácsi, Investigation of intermetallic compounds in Sn-Cu-Ni lead-free solders, Arch. Metall. Mater. 60 (2015) 1511–1515, https://doi.org/10.1515/amm-2015-0163.
[67] V. Sharma, C. Chotia, Tarachand, V. Ganesan, G.S. Okram, Influence of particle size and dielectric environment on the dispersion behaviour and surface plasmon in nickel nanoparticles, Phys. Chem. Chem. Phys. 19 (2017) 14096–14106, https://doi.org/10.1039/c7cp01769c.
[68] O.A. Yeshchenko, V. Kozachenko, A.V. Tomchuk, Surface plasmon resonance in "monolayer of Ni nanoparticles/dielectric spacer/Au (Ni) film" nanostructure: tuning by variation of spacer thickness, Ukrainian J. Phys. 63 (2018) 386–395, https://doi.org/10.15407/ujpe63.5.386.
[69] P. Liu, H. Wang, X. Li, M. Rui, H. Zeng, Localized surface plasmon resonance of Cu nanoparticles by laser ablation in liquid media, RSC Adv. 5 (2015) 79738–79745, https://doi.org/10.1039/C5RA14933A.
[70] T. Wu, Y. Kou, H. Zheng, J. Lu, N.R. Kadasala, S. Yang, C. Guo, Y. Liu, M. Gao, A novel Au@Cu_2O-Ag ternary nanocomposite with highly efficient catalytic performance: towards rapid reduction of methyl orange under dark condition, Nanomaterials 10 (48) (2020) 1–14, https://doi.org/10.3390/nano10010048.
[71] K.S.W. Sing, D.H. Everett, R.A.W. Hall, L. Moscou, R.A. Pierotti, J. Rouquérol, T. Siemieniewska, Reporting physisorption data for gas/solid systems with special reference to the determination of surface area and porosity, Pure Appl. Chem. 57 (1985) 603–619, https://doi.org/10.1351/pac198557040603.